Physica B 406 (2011) 2532–2539

Contents lists available at ScienceDirect

Physica B

journal homepage: www.elsevier.com/locate/physb

$BiFeO_3$ ceramic matrix with Bi_2O_3 or PbO added: Mössbauer, Raman and dielectric spectroscopy studies

H.O. Rodrigues [a,b], G.F.M. Pires Junior [a,b], A.J.M. Sales [a,b], P.M.O. Silva [a,b], B.F.O. Costa [c], P. Alcantara Jr[d], S.G.C. Moreira [d], A.S.B. Sombra [b,*]

[a] Departamento de Engenharia de Teleinformática-UFC, Caixa Postal 6007, CEP 60755-640, Fortaleza, Ceará, Brazil
[b] Laboratório de Telecomunicações e Ciência e Engenharia dos Materiais (LOCEM), Caixa Postal 6030, CEP 60455-760, Fortaleza, Ceará, Brazil
[c] CEMDRX, Physics Department, University of Coimbra 3004-516 Coimbra, Portugal
[d] Departamento de Fisica, Universidade Federal do Pará, Brazil

ARTICLE INFO

Article history:
Received 10 November 2010
Accepted 19 March 2011
Available online 29 March 2011

Keywords:
Inorganic compounds
Mössbauer spectroscopy
Raman spectroscopy
Electrical properties

ABSTRACT

In this paper Mössbauer, Raman and dielectric spectroscopy studies of $BiFeO_3$ (BFO) ceramic matrix with 3 or 10 wt% of Bi_2O_3 or PbO added, obtained through a new procedure based on the solid-state method, are presented. Mössbauer spectroscopy shows the presence of a single magnetically ordered phase with a hyperfine magnetic field of 50 T. Raman spectra of BFO over the frequency range of 100–900 cm^{-1} have been investigated, at room temperature, under the excitation of 632.8 nm wavelength in order to evaluate the effect of additives on the structure of the ceramic matrix. Detailed studies of the dielectric properties of $BiFeO_3$ ceramic matrix like capacitance (C), dielectric permittivity (ε) and dielectric loss ($\tan\delta$), were investigated in a wide frequency range (1 Hz–1 MHz), and in a temperature range (303–373 K). The complex impedance spectroscopy (CIS) technique, showed that these properties are strongly dependent on frequency, temperature and on the added level of impurity. The temperature coefficient of capacitance (TCC) of the samples was also evaluated. The study of the imaginary impedance ($-Z''$) and imaginary electric modulus (M'') as functions of frequency and temperature leads to the measurement of the activation energy (E_{ac}), which is directly linked to the relaxation process associated with the interfacial polarization effect in these samples.

1. Introduction

Multiferroic materials have attracted considerable attention from researchers around the world, associated with their potential for applications in innovative technological devices, such as electromagnetic devices, optoelectronics and spintronics [1]. The electric control on the ferromagnetic properties of these materials opens a very rich field of research for future innovative devices, with impact on magnetic data storage, spintronics, and high-frequency magnetic devices. The perspective to control charges by applied magnetic fields and spins by applied voltages, and using this to construct new forms of multifunctional devices, drives the search for these materials [2]. There are empirically a few multiferroic materials [3], and $BiFeO_3$ (a perovskite-type material) has attracted continuous attention among the multiferroics because it shows both ferroelectric and antiferromagnetic ordering at room temperature (Curie temperature $T_C \sim 1100$ K, Néel temperature $T_N \sim 640$ K), with a large ferroelectric polarization at 300 K in thin films [4–9].

Several investigations of $BiFeO_3$ (BFO) at room temperature by Mössbauer spectroscopy have been published [10,11]. We have used Mössbauer spectroscopy at room temperature to achieve a detailed understanding of the magnetic behavior of these ceramics and the effect of the addition of Bi_2O_3 and PbO in the hyperfine parameters.

To investigate lattice properties, magnetic ordering and structural phase transitions in solids Raman spectroscopy is a powerful tool, and its applications in multiferroic materials have been discussed [4,12–14]. Raman spectra of BFO over the frequency range of 100–900 cm^{-1} have been investigated at room temperature under the excitation of 632.8 nm wavelength (1.96 eV). Raman spectroscopy was used to evaluate the effect of additives on the structure of the $BiFeO_3$ ceramic matrix with 3 and 10 wt% of Bi_2O_3 or Bo added. All these data may provide useful information for better understanding the relationship between magnetic properties and structure of $BiFeO_3$ with Bi_2O_3 and Bo addition.

Detailed studies of the dielectric properties of $BiFeO_3$ ceramic matrix like capacitance (C), dielectric permittivity (ε) and dielectric loss ($\tan\delta$), were investigated in a wide frequency (1 Hz–1 MHz),

* Corresponding author. Tel.: +55 85 33669334; fax +55 85 33669332.
E-mail address: sombra@ufc.br (A.S.B. Sombra).
URL: http://www.locem.ufc.br (A.S.B. Sombra).

0921-4526 © 2011 Elsevier B.V. Open access under the Elsevier OA license.
doi:10.1016/j.physb.2011.03.050

and in a temperature range (303–373 K). The complex impedance spectroscopy technique, showed that these properties are strongly dependent on frequency, temperature and on the added level of impurity. The temperature coefficient of capacitance (TCC) and activation energy (E_{ac}) of the samples were also evaluated.

2. Experimental procedure

2.1. Sample preparation

$BiFeO_3$ (BFO) samples were prepared through the solid-state reaction method, exactly according to the recent fabrication procedure described in Ref. [15]. Reagents and oxides were accurately weighed in stoichiometric amounts of Bi_2O_3 (Aldrich, 99.9%) and Fe_2O_3 (Aldrich, 99.0%). Previously to the first heat treatment, high-energy ball milling of the homogeneous powder mixture was conducted in a planetary ball mill (Fritsch Pulverisette 6) for 1 h. The mixtures were then calcinated in conventional controlled furnaces. After calcination Bi_2O_3 (3 and 10 wt%) or PbO (3 and 10 wt%) was added to the samples, resulting in five different samples named BFO-0 (no adding), BFO-Bi3P, BFO-Bi10P, BFO-Pb3P and BFO-Pb10P. Polyvinyl alcohol (PVA) was also added (about 5 wt%) as a binder to all samples except BFO-0. The pellets were sintered at 810 °C for 1 h in air, as described in Ref. [15].

2.2. Mössbauer spectroscopy measurements

^{57}Fe Mössbauer spectra was registered at room temperature with a 25 mCi Co/Rh source in conventional transmission geometry. The drive was a WISSEL operating in a triangular mode. The fitting of the spectra was carried out with WINNORMOS programme by a set of Lorentzian lines using a least-square minimum procedure. The isomer shifts are given relative to α-Fe.

2.3. Raman spectroscopy measurements

Raman scattering was performed using a He–Ne laser source at 632.8 nm (17 mW), micro-Raman spectrometer iHR 320 (Horiba; width (resolution)∼0.06 nm) and a detector Synapse charge-coupled-device CCD camera cooled to −77 °C with Peltier, with USB interface.

2.4. Dielectric measurements

Silver paint electrode was coated on both polished surfaces of the sintered disks with a parallel-plate capacitor arrangement. The sintered pellets were dried at 120 °C for 20 min, for better contact of the electrodes. The complex impedances of the samples were measured in atmospheric air using a system of acquisition of data that was mounted and consists of the use of an electrical oven model equipped with a COEL controller model HW4200 to an impedance analyzer Solartron model SI 1260 controlled by a personal computer. The temperature was tuned from 30 (∼303) to 100°C (∼373 K) with a stability of 0.1 °C in air. The measurements were carried out with an applied potential of 500 mV in the frequency range from 1 Hz to 1 MHz.

The ε' value was calculated from the capacitance value $C(f)$, the thickness (t) of pellets, and the area (A) of the electrodes. $C(f)$ was obtained through the electrical impedance $Z(f)$, and it is a complex quantity whose real and imaginary parts correspond directly to the real and imaginary components of the complex permittivity:

$$C(f) = C'(f) - jC''(f) = \left(\frac{A}{t}\right)\left[\varepsilon'(f) - j\varepsilon''(f)\right]. \quad (1)$$

Another important quantity required for engineering applications is the loss angle δ by which the phase of the electric flux density $D(f)$ lags behind the driving voltage $E(f)$. The tangent of this loss angle is given by:

$$\tan\delta = C''(f)/C'(f) = \varepsilon''(f)/\varepsilon'(f) \quad (2)$$

The practical significance of tan δ is that it represents the ratio of the energy dissipated per radian in the dielectric to the energy stored at the peak of the polarization.

One practical advantage of tan δ as a figure of merit of a dielectric material consists in its independence of the geometry of the sample—it is the ratio of two parameters containing the same geometrical factor [16].

The temperature coefficient of capacitance (TCC) was calculated by the following equation:

$$TCC = [(CT_2 - CT_1)]/CT_1[(T_2 - T_1)], \quad (3)$$

where CT_1 is the measured capacitance at T_1 (where T_1 is 30 °C) and CT_2 is the measured capacitance at $T_2 = 100$ °C [16].

In order to study the frequency and temperature dependences of the interfacial polarization effect, which generates electric charge accumulation around the ceramic particles, displacing relaxation peaks, electrical modulus (M) was used. The real and imaginary parts of the electrical modulus, M' and M'', respectively they can be calculated as fallows [17]:

$$M = \frac{1}{\varepsilon^*} = \frac{1}{(\varepsilon' - j\varepsilon'')} = M' + jM'', \quad (4)$$

$$M' = \frac{\varepsilon'}{(\varepsilon\prime)^2 + (\varepsilon'')^2}, \quad (5)$$

$$M'' = \frac{\varepsilon''}{(\varepsilon\prime)^2 + (\varepsilon'')^2}. \quad (6)$$

The activation energy (E_{ac}) of the relaxation was calculated starting from the values of the maximum frequencies in each curve of $M''(f)$ as a function of temperature for the samples with PbO added, and from the values of the maximum frequencies in each curve of $Z''(f)$ as a function of the temperature for the samples with Bi_2O_3 added. Considering that the process is activated by temperature in:

$$f = f_0 e^{(-E_{ac}/kT)}, \quad (7)$$

where f is the maximum frequency in the samples (at temperature T), f_0 is the equilibrium pre-exponential frequency representing typical atomic approach [18], k is the Boltzmann constant, E_{ac} is the activation energy and T is the temperature (K).

3. Results and discussion

Figs. 1 and 2 show the room temperature Mössbauer spectra of $BiFeO_3$ samples. The spectra were fitted with one sextet and two doublets. The hyperfine parameters were obtained in a fitting procedure and are shown in Table 1. The BFO–0 (reference sample) has almost the same hyperfine parameters as the ones obtained in early reports [19,20]. This sample shows the presence of a single phase, magnetically ordered, with a hyperfine magnetic field of about 50 T. The presence of two other doublets, which arise from a single phase (or phases), do not seem to be magnetically ordered, was also detected. The Mössbauer parameters of these doublets match closely with those of $Bi_2Fe_4O_9$ [19,20]. In our case the total absorption area of the doublets is about 60%, while the area found by Maurya et al. [19] is about 50%.

In all the studied samples (added with Bi_2O_3 and with PbO) the six-line spectrum remains and the parameters are similar to those

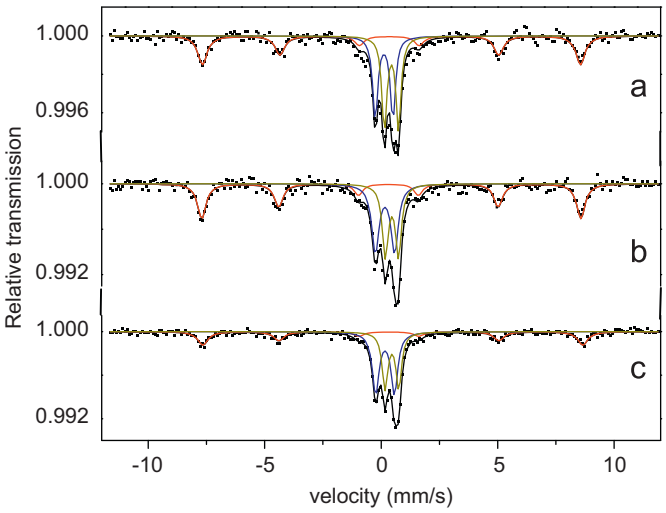

Fig. 1. Mössbauer spectra of $BiFeO_3$ samples: (a) BFO-0; (b) BFO–Bi3P and (c) BFO–Bi10P.

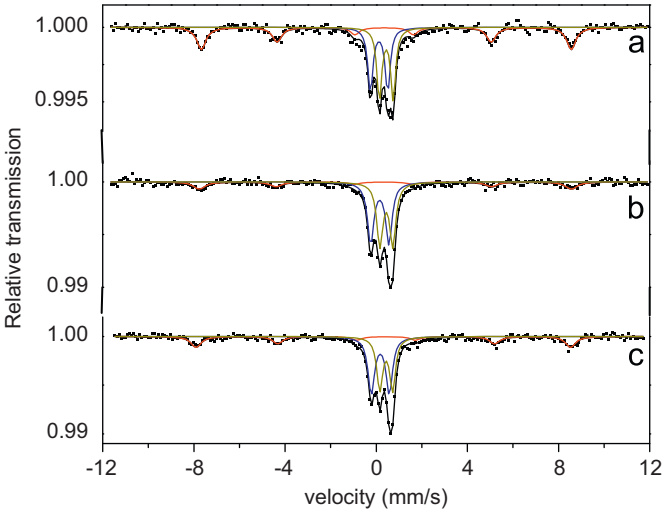

Fig. 2. Mössbauer spectra of $BiFeO_3$ samples: (a) BFO-0; (b) BFO–Pb3P and (c) BFO–Pb10P.

Table 1
Hyperfine parameters obtained by fitting of the two sextets model to the $BiFeO_3$ Mössbauer spectra.

Sample	IS (mm/s)	QS (mm/s)	Width (mm/s)	H (T)	%
BFO–0	0.40(1)	0.09(1)	0.49(1)	50.3(1)	37.5
	0.12(2)	0.76(1)	0.27(1)	–	30.0
	0.44(2)	0.60(1)	0.26(1)	–	32.5
BFO–Bi3P	0.37(1)	0.13(1)	0.45(2)	50.4(2)	39.7
	0.16(1)	0.83(1)	0.38(1)	–	32.5
	0.46(1)	0.57(1)	0.31(1)	–	27.8
BFO–Bi10P	0.42(1)	0.17(1)	0.53(1)	50.5(1)	27.3
	0.16(1)	0.80(2)	0.35(1)	–	41.0
	0.46(1)	0.59(2)	0.30(1)	–	31.7
BFO–Pb3P	0.37(1)	0.07(1)	0.64(2)	50.6(1)	18.4
	0.16(1)	0.80(1)	0.34(1)	–	41.2
	0.44(1)	0.57(1)	0.32(1)	–	40.4
BFO–Pb10P	0.37(1)	0.12(1)	0.54(1)	50.8(1)	24.8
	0.18(1)	0.79(2)	0.34(1)	–	40.5
	0.44(1)	0.56(2)	0.31(1)	–	34.7

of pure BFO, so the iron in the doped samples has the same valence as in BFO. For all samples the $Bi_2Fe_4O_9$ phase remains, however with an increase in the Lorentzian line width at half maximum (FWHM), indicating that the environment around iron ions present a distribution.

The total absorption area of the magnetic phase does not remain constant in the doped samples, increasing or decreasing according to some conditions, as observed in the Table 1.

Fig. 3 shows the Raman spectrum at room temperature for the sample BFO–0. Group theory provides 13 Raman active modes ($\Gamma_{\text{Raman, R3c}}=4A_1+9E$) in a $BiFeO_3$ crystal structure—rhombohedral, space group R3c [21,22] and 5 Raman and IR-inactive modes [23]. These active modes were observed more recently in single crystals by Fukumara et al. [4]. As previously indicated by X-ray diffraction in our previous work [15], our sample has the same crystalline structure with regard to the $BiFeO_3$ phase. Singh et al. [12] reported 10 Raman active modes in BFO thin films of epitaxial orientation with R3c structure, including A_1-1, A_1-2 and A_1-3 modes at 136, 168 and 211 cm^{-1}, respectively, with strong scattering intensity, and the A_1-4 mode at 425 cm^{-1}, with weak scattering intensity beyond six E modes at 275, 335, 365, 456, 549 and 597 cm^{-1}, with average intensity of scattering. Fukumura et al. [4] found all 13 modes predicted by the group theory. Yuan et al. [24] also report seeing only 10 Raman active modes in BFO films. Kothari et al. [14] found 13 Raman active modes. In the present study we found 10 Raman active modes in our BFO-0 reference sample. Table 2 lists the values found in the literature and in this work only for the ceramic sample BFO–0. The subtle difference in

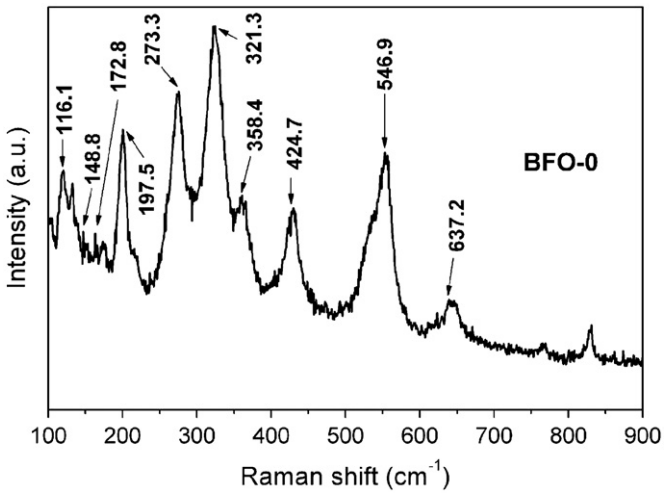

Fig. 3. Raman spectra of $BiFeO_3$ sample (BFO-0) at room temperature (~300 K).

Table 2
Comparison between the Raman mode frequency (cm^{-1}) obtained in this study and in the literature (for reference sample BFO–0).

Raman mode (cm^{-1})	This work	Yang et al. [22]	Kothari et al. [14]	Fukumura et al. [4]	Singh et al. [12]	Yuan et al. [23]
A_1-1	148.8	139	135.15 ± 1.38	147	136	152.6
A_1-2	172.8	172	167.08 ± 0.34	176	168	177.5
A_1-3	197.5	217	218.11 ± 0.45	227	211	224.2
A_1-4	424.7	470	430.95 ± 16.69	490	425	–
E	273.3	275	255.38 ± 0	265	275	270
E	321.3	307	283.0 ± 0	279	335	298.8
E	358.4	345	351.55 ± 8.66	351	365	354.9
E	–	369	321.47 ± 3.76	375	–	–
E	–	429	467.6 ± 2.46	437	456	473.3
E	546.9	521	526.22 ± 2.57	473	549	554.3
E	637.2	613	598.84 ± 1.99	525	597	618.3
E	–	–	71.39 ± 0.11	77	–	–
E	116.1	–	98.36 ± 3.11	136	–	–

some of the peak positions observed by different researchers can be attributed to the details of preparation of each sample. It is known that sample preparation methods influence the stoichiometry of oxygen. Changes in the binding of oxygen and in disorderare expected to observed which is reflected in the frequencies of vibration modes involving oxygen [14].

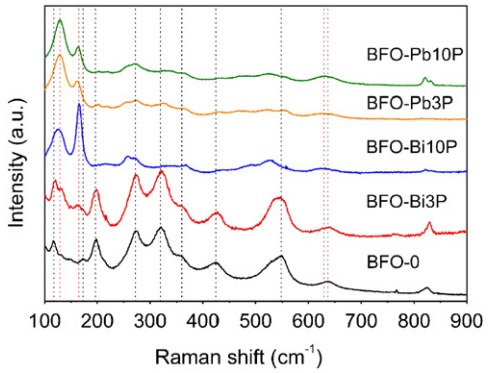

Fig. 4. Raman spectra of $BiFeO_3$ samples with Bi_2O_3 added or with PbO at room temperature (~300 K). The 10 Raman active modes found in the reference sample are indicated by black dotted lines. Other observed modes in samples with addtion are indicated by red dotted lines.

In Fig. 4 shows Raman spectra of $BiFeO_3$ samples with either Bi_2O_3 or PbO at room temperature (~300 K). In BFO–Bi3P sample shift of the peaks was not observed, indicating that the stoichiometry was not significantly changed. With increasing concentration of bismuth oxide for 10 wt%, there is a decrease in intensity of several peaks: thus one observes the apparent disappearance of some Raman modes in the configuration of the considered polarization. On adding PbO, we observed changes in Raman spectra. Several peaks disappear, indicating that with the addition of lead oxide new modes are generated. The peak at 273.3 cm^{-1} has decreased in intensity compared to the reference sample. New peaks appear at 129.3, 163.9 ,and 631.5 cm^{-1} (red dotted lines). The peak at 820.8 cm^{-1} is probably indicative of a resonant mode. Usually it the origin of the high-frequency peaks in the Raman spectra is attributed to electronic Raman scattering or high-order phonon scattering [23 and references therein].

Figs. 5 and 6 presents the dielectric permittivity, ε' ($=\varepsilon'_r$) and loss respectively, of $BiFeO_3$ samples, all depending on frequency and temperature. Regarding BFO-0 sample it is observed that the

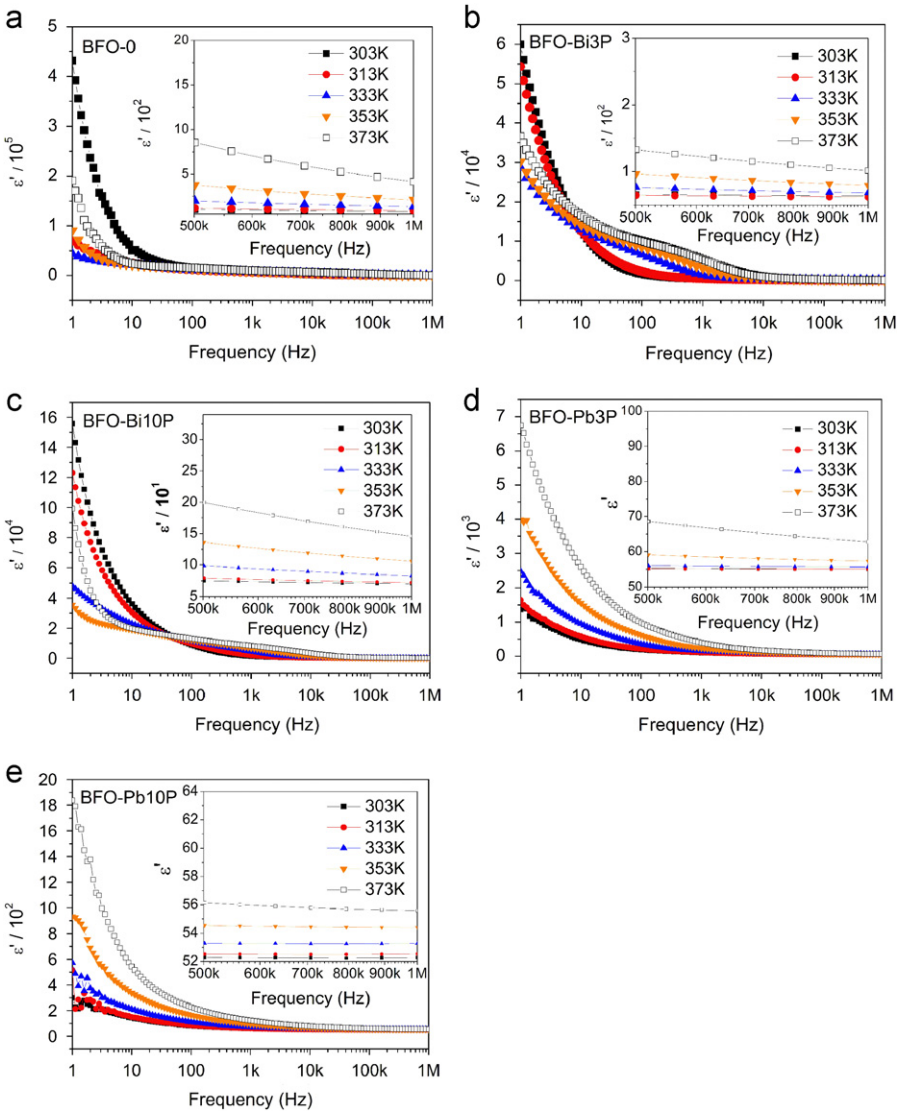

Fig. 5. Dielectric permittivity, ε', of $BiFeO_3$ samples: (a) BFO-0; (b) BFO–Bi3P; (c) BFO–Bi10P; (d) BFO–Pb3P and (e) BFO–Pb10P, all depending on the frequency and temperature.

addition of bismuth oxide promotes a relative reduction in the value of dielectric permittivity, but this reduction was even more significant when lead oxide was added. At low frequencies , the samples BFO-0, BFO–Bi3P and BFO–Bi10P have higher values of permittivity, which drcrease with increasing temperature, acquiring intermediate values at the final temperature of 373 K. Moreover, with respect to the BFO–Pb3P and BFO–Pb10P samples, with the increase in the temperature there is an increase in permittivity at low frequencies. The Maxwell–Wagner model provides for the behavior of complex conductivity in heterogeneous systems with two or more phases [25]. In a heterogeneous system, if the region of continuity of the grain boundary occupies a small volume, the spectrum of impedance ($-Z''$ *versus* Z') provides better visualization of the semicircles in the plan. It was this behavior we observe in the sample BFO–0 and in other samples doped with Bi_2O_3. There is a probable relationship between the behavior of grain boundary, as described by the model, and the appearance of the peaks of Z'' as functions of frequency and temperature, and has been presented in Fig. 7(a)–(e). Otherwise, if the region of grain boundary occupies a large volume, the graph of the modulus ($M^*=1/\varepsilon^*$) M'' *versus* M', provides better information about the semicircles, due to minimizing of the effect observed in the capacitance of electrode–sample interface and emphasizing the small features at high frequencies. We can see that this second type of behavior applies to the samples with PbO addtion, suggesting once again correspondingly that there is a probable relationship between the behavior of grain boundary and the appearance of the peaks of M'' as a function of frequency and temperature, as has been presented in Fig. 7(d)–(e). Regarding the AC conductivity, a former study [15] showed that the samples with lead oxide have conductivity values relatively very small, unlike the samples adding with bismuth oxide addtion.

Fig. 6 presents the dielectric loss (tan δ) of $BiFeO_3$ samples, all depending on frequency and temperature. In the graphs of loss tangent of the samples BFO-0, BFO–Bi3P ,and BFO–Bi10P, one notes the presence of peaks. The presence of such peaks is related to the appearance of peaks in the graph of the imaginary part of impedance ($-Z''$) versus frequency, as we can see in Fig. 7(a)–(c). But in the samples doped with lead, this behavior is not observed. In this case, in the graphs of loss tangent, no peaks were observed. Now, the absence of these peaks in the graph of loss tangent will result in the appearance of peaks only in the graph of the imaginary electric modulus (M'') versus frequency, as we can see in Fig. 7(d)–(e). These behaviors should be related to the

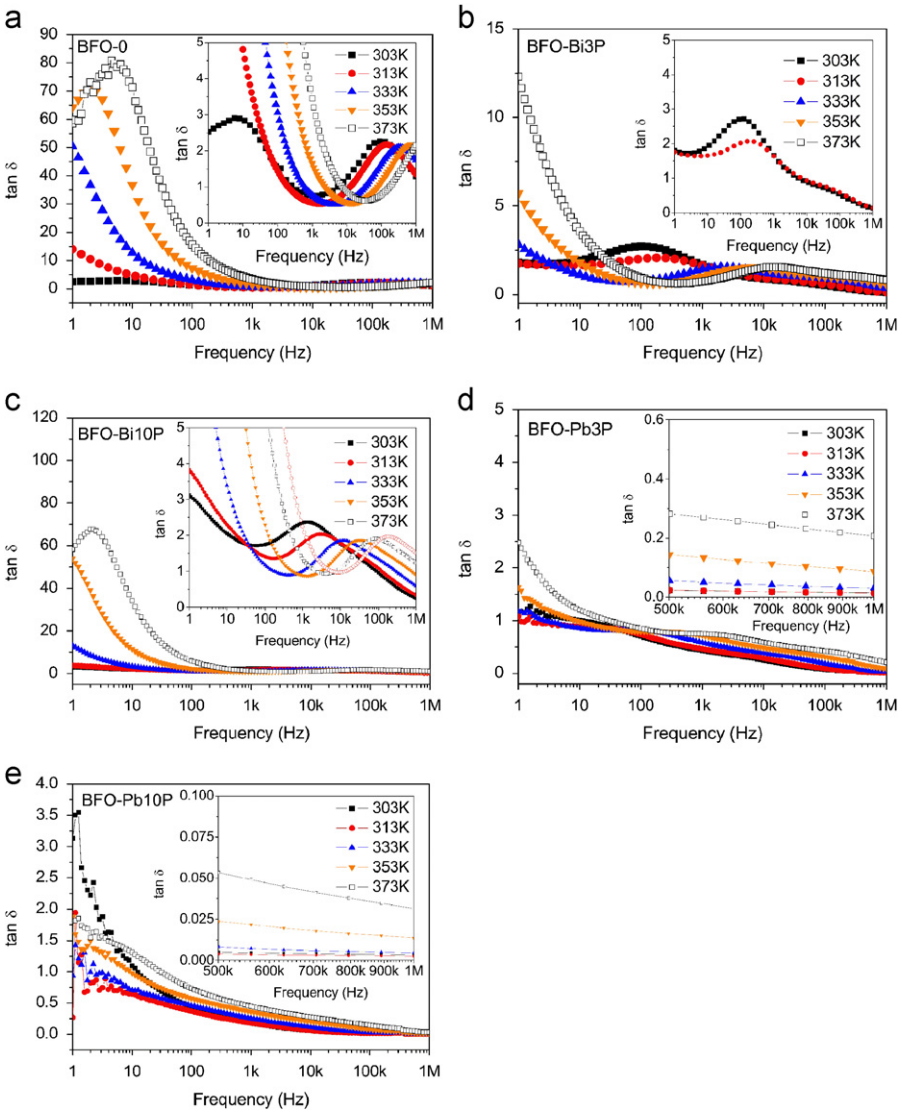

Fig. 6. Dielectric loss (tan δ) of $BiFeO_3$ samples: (a) BFO–0; (b) BFO–Bi3P; (c) BFO–Bi10P; (d) BFO–Pb3P and (e) BFO–Pb10P, all depending on frequency and temperature.

inhomogeneity of the samples and the presence of impurities within the structure of the material.

In Table 3 we have the values for the dielectric permittivity (ε'_r) and loss tangent ($\tan\delta$) at 1 MHz for all samples and temperatures. We can observe that the BFO–Pb10P is presenting ε'_r value equal to 53, with the lowest value for the loss (2.54×10^{-3}) at 313 K (~25 °C). With increase in temperature, starting from 313 K, BFO–Pb10P always presents low value of $\tan\delta$ for all samples and temperatures. BFO–Pb10P keeps its permittivity values relatively stable, over the evaluated temperature range, showing a degree of non-dependence

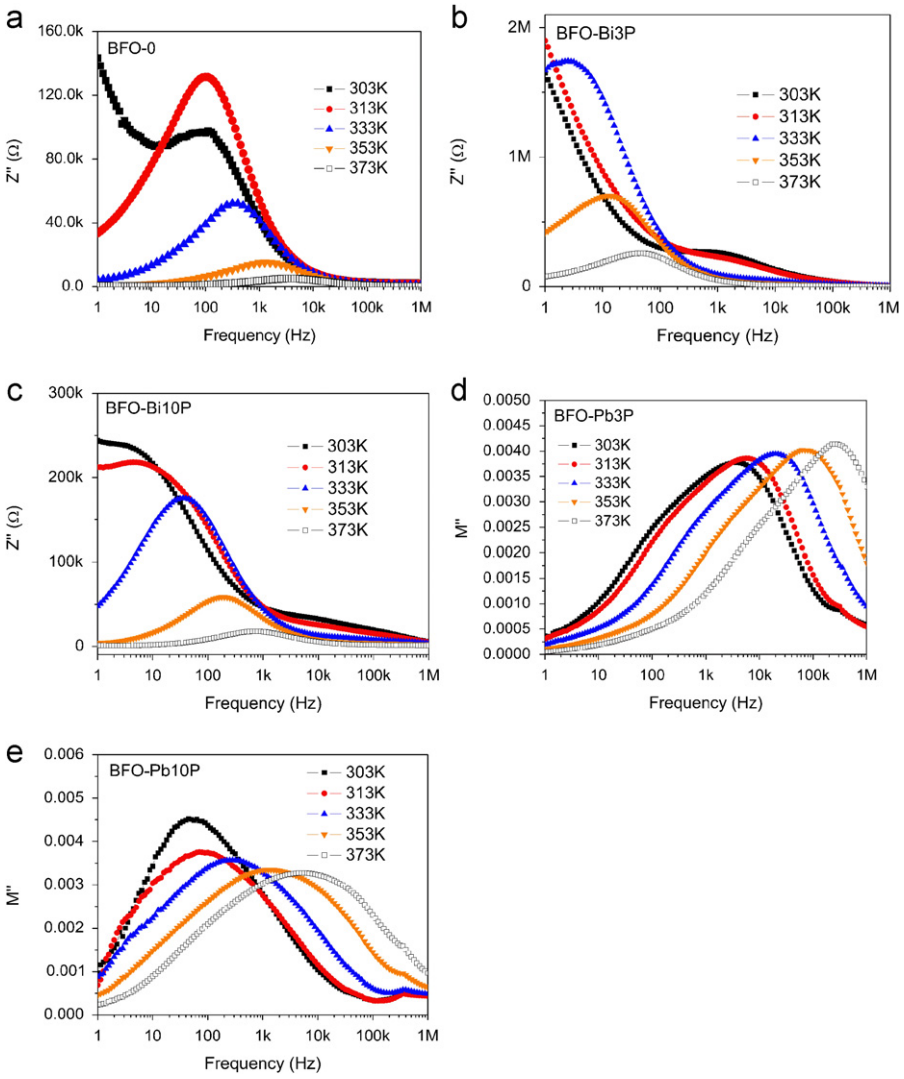

Fig. 7. Imaginary impedance (Z'') as functions of frequency and temperature: (a) BFO-0; (b) BFO–Bi3P; (c) BFO–Bi10P; appearance and displacement of the peaks of M'' as functions of frequency and temperature: (d) BFO–Pb3P and (e) BFO–Pb10P.

Table 3
Dielectric permittivity (ε') and dielectric loss ($\tan\delta$) of the BFO samples sintered at 810 °C/1 h for some temperatures.

Samples	BFO-0	BFO–Bi3P	BFO–Bi10P	BFO–Pb3P	BFO–Pb10P
T=303 K					
ε'_r	**79**	**63**	**70**	**55**	**52**
tan δ	$\mathbf{1.29\times10^{0}}$	$\mathbf{1.27\times10^{-1}}$	$\mathbf{2.50\times10^{-1}}$	$\mathbf{1.45\times10^{-2}}$	$\mathbf{3.44\times10^{-3}}$
***T*=313 K**					
ε'_r	**90**	**62**	**72**	**55**	**53**
tan δ	$\mathbf{1.35\times10^{0}}$	$\mathbf{1.40\times10^{-1}}$	$\mathbf{3.32\times10^{-1}}$	$\mathbf{1.36\times10^{-2}}$	$\mathbf{2.54\times10^{-3}}$
***T*=333 K**					
ε'_r	**137**	**68**	**83**	**55**	**53**
tan δ	$\mathbf{1.73\times10^{0}}$	$\mathbf{3.62\times10^{-1}}$	$\mathbf{5.87\times10^{-1}}$	$\mathbf{3.03\times10^{-2}}$	$\mathbf{4.64\times10^{-3}}$
***T*=353 K**					
ε'_r	**213**	**79**	**106**	**57**	**54**
tan δ	$\mathbf{2.15\times10^{0}}$	$\mathbf{5.87\times10^{-1}}$	$\mathbf{9.02\times10^{-1}}$	$\mathbf{8.69\times10^{-2}}$	$\mathbf{1.36\times10^{-2}}$
***T*=373 K**					
ε'_r	**416**	**101**	**146**	**63**	**55**
tan δ	$\mathbf{2.16\times10^{0}}$	$\mathbf{8.14\times10^{-1}}$	$\mathbf{1.23\times10^{0}}$	$\mathbf{2.06\times10^{-1}}$	$\mathbf{3.16\times10^{-2}}$

For all samples, f=1 MHz.

Table 4
Temperature coefficient of capacitance (TCC) and activation energy (E_{ac}) of the samples.

Sample	BFO-0	BFO–Bi3P	BFO–Bi10P	BFO–Pb3P	BFOPb10P
TCC (ppm/°C), f=1 Hz	−7982	−5560	−5197	56157	73583
TCC (ppm/°C), f=10 Hz	−7466	4135	−6427	62614	39054
TCC (ppm/°C), f=100 Hz	838	70958	6874	59511	24878
TCC (ppm/°C), f=1 kHz	5394	166092	74103	40553	14297
TCC (ppm/°C), f=10 kHz	26159	69663	148477	22404	6666
TCC (ppm/°C), f=100 kHz	154712	33536	52391	9637	2163
TCC (ppm/°C), f=1 MHz	60436	8520	15254	1998	913
E_{ac} (eV)	0.61	0.77	0.85	0.58	0.72

of permittivity on temperature. BFO–0 showed the highest variation of permittivity with increase in temperature, with a value of 416 at a temperature of 373 K (~100 °C). In parallel, the dielectric losses of this sample were also the largest in the whole temperature range, reaching a maximum value of 2.16. There is a direct relationship between the behavior of the temperature dependence of permittivity and dielectric losses with the values obtained for temperature coefficient of capacitance (TCC), since the capacitance of the sample depends on these intrinsic parameters of the dielectric.

Table 4 shows the calculated values of the temperature coefficient of capacitance (TCC), according to Eq. (3), in the range of 30–100 °C, for some frequencies, and summarizes the values of activation energy (E_{ac}) found, according to Eq. (7). The BFO-0 sample showed negative values of TCC at low frequencies, which tells us, in this case, the increase in temperature reduces the capacitance of the sample. In this sample, between 100 Hz and 100 kHz, we have positive values of TCC, thus positive changes in frequency imply a positive change in capacitance values; Between 10 and 100 Hz a frequency is expected where TCC is practically zero. The maximum value of TCC (absolute value) for this reference sample occurs around the frequency of 100 kHz. The BFO–Bi3P sample exhibits similar behavior when compared to the reference sample, but with negative TCC only near the frequency of 1 Hz. Addition of 3 wt% Bi_2O_3 made the maximum recorded value of TCC occur at a lower frequency, i.e. 1 kHz. Also observed in this sample is the largest absolute value of TCC, 166,092 ppm/°C at 1 kHz. For BFO–Bi10P, the zero crossing is likely to occur between 10 and 100 Hz. In samples with addition of PbO, we have found starting values of positive and relatively high TCC values. The lower the frequency, the more susceptible to temperature changes the capacitances of these samples. The lowest value found (absolute value) was 838 ppm/°C for the sample BFO-0 at a frequency of 100 Hz, which shows a good stability of capacitance in the temperature range of 30–100 °C. Ideally, the value of TCC should be as close to zero, minimizing the effects of changing ambient temperature on the capacitance. The reduction of porosity and the addition of other material with TCC < 0, to form a composite, are a possible way to obtain TCC ~ 0, at the desired frequency. However, large variations in capacitance may be interesting for the design of sensitive temperature sensors.

For pure phases E_{ac} is identified with the energy to form defects together with the energy to move them. If defects are introduced by doping, then the thermal energy is required only to move them and E_{ac} is correspondingly lower [26]. Khomchenko et al. [27] have performed measurements in the $Bi_{0.8}Pb_{0.2}FeO_3$ system obtaining an activation energy $E_\sigma \sim 0.65$ eV, which is quite typical for oxygen vacancies-related conductivity. This value is in good agreement with the value obtained for our BFO-0 sample, indicating that in the frequency/temperature dependencies of the dielectric permittivity and loss factor, the oxygen vacancies-related dipoles follow the alternating field at low frequencies, providing high values of ε', but lag behind the field in the high-frequency range, as presented in our previous work [15]. In our measurements, made in doped and undoped phases, it is observed that the addition of 10 wt% Bi_2O_3, in relation to the addition of 3 wt% Bi_2O_3, caused an increase (of about ~10%) in the value of activation energy, which probably indicates that the sample BFO–Bi10P will require more energy in the process of displacement of charge carriers. As for the addition of PbO, there was also an increase in the value of activation energy (of about ~24%), between BFO–Pb3P and BFO–Pb10P.

4. Conclusion

Polycrystalline $BiFeO_3$ (BFO) ceramic matrix with 3 or 10 wt% Bi_2O_3 or PbO added has been prepared by the solid-state method. The observed hyperfine parameters, determined from Mössbauer spectroscopy, match closely with the reported data elsewhere. The iron in the added samples has the same valence as in our BFO reference sample. The presence of the $Bi_2Fe_4O_9$ phase was detected in our samples, resulting probably of the manufacturing process of the samples. We found 10 Raman active modes in our BFO-0 reference sample. For the 3 wt% Bi_2O_3 added samples, shift of the Raman peaks was not observed, indicating that the stoichiometry was not significantly changed. With increasing concentration of bismuth oxide to 10 wt%, there is a decrease in intensity of several peaks, and apparent disappearance of some Raman modes was observed. On adding PbO, several peaks disappear, indicating that with the addition of lead oxide some modes are degenerated. It is also observed that the addition of bismuth oxide promotes a relative reduction in the value of dielectric permittivity, but this reduction was even more significant when lead oxide was added. For the lead oxide added samples, the increase in temperature lead to an increase in permittivity, at low frequencies. We obtain the temperature coefficient of capacitance (TCC) and activation energy (E_{ac}). The lowest value of TCC found was 838 ppm/°C for the sample BFO-0 at a frequency of 100 Hz, which shows a good stability of capacitance in the temperature range of 30–100 °C. Our results may provide useful information for understanding the relationship between the lattice structure and electronic and magnetic ordering in this specific category of multiferroic ceramic materials.

Acknowledgment

This work was partly sponsored by **CNPq** and **CAPES** (Brazilian agencies).

References

[1] H. Béa, M. Bibes, S. Fusil, K. Bouzehouane, E. Jacquet, K. Rode, P. Bencok, A. Barthélémy., Phys. Rev. B 74 (2006) 020101 R.
[2] S.W. Cheong, M. Mostovoy, Nature Mater 6 (2007) 13.
[3] W. Eerenstein, N.D. Mathur, J.F. Scott, Nat. 442/17 (2006) 759.

[4] H. Fukumura, S. Matsui, H. Harima, T. Takahashi, T. Itoh, K. Kisoda, M. Tamada, Y. Noguchi, M. Miyayama, J. Phys.: Condens. Matter 19 (2007) 365224.
[5] H. Fukumura, H. Harima, K. Kisoda, M. Tamada, Y. Noguchi, M. Miyayama, J. Magn. Magn. Mater. 320 (2008) 548.
[6] G.A. Smolenski, V.M. Yudin, Sov. Phys. JETP 16 (1963) 622.
[7] I.G. Ismailzade, Phys. Status Solidi B 46 (1971) K39.
[8] J. Wang, J.B. Neaton, H. Zheng, V. Nagarajan, S.B. Ogale, B. Liu, D. Viehland, V. Vaithyanathan, D.G. Schlom, U.V. Waghmare, N.A. Spaldin, K.M. Rabe, M. Wuttig, R. Ramesh, Science 299 (2003) 1719.
[9] D. Lebeugle, A. Mougin, M. Viret, D. Colson, L. Ranno, Phys. Rev. Lett. 103 (2009) 257601.
[10] S.A. Ivanov, P. Nordblad, R. Tellgren, T. Ericsson, S.K. Korchagina, L.F. Rybakova, A. Hewat, Solid State Sci. 10 (2008) 1875.
[11] I.A. Santos, L.F. Cotica, S.N. de Medeiros, Ferroelectrics 338 (2006) 233.
[12] M.K. Singh, H.M. Jang, S. Ryu, M.H. Jo, Appl. Phys. Lett. 88 (2006) 042907.
[13] R. Haumont, J. Kreisel, P. Bouvier, F. Hippert, Phys. Rev. B 73 (2006) 132101.
[14] D. Kothari, V.R. Reddy, V.G. Sathe, A. Gupta, A. Banerjee, A.M. Awasthi, J. Magn. Magn. Mater. 320 (2008) 548.
[15] H.O. Rodrigues, G.F.M. Pires Junior, J.S. Almeida, E.O. Sancho, A.C. Ferreira, M.A.S. Silva, A.S.B. Sombra, J. Phys. Chem. Solids 71 (2010) 1329.
[16] F.N.A. Freire, M.R.P. Santos, F.M.M. Pereira, R.S.T.M. Sohn, J.S. Almeida, A.M.L. Medeiros, E.O. Sancho, M.M. Costa, A.S.B. Sombra, J. Mater. Sci.: Mater. Electron. 20 (2009) 149.
[17] A.K. Jonscher, Dielectric Relaxation in Solids, Chelsea Dielectric Press, London, 1983.
[18] A.K. Batra, J.R. Currie, M.A. Alim, M.D. Aggarwal, J. Phys. Chem. Solids 70 (2009) 1142.
[19] D. Maurya, H. Thota, A. Garg, B. Pandey, P. Chand, H.C. Verma, J. Phys.: Condens. Matter 21 (2009) 026007.
[20] L.Y. Wang, D.H. Wang, H.B. Huang, Z.D. Han, Q.Q. Cao, B.X. Gu, Y.W. Du, J. Alloys Compd. 469 (2009) 1.
[21] P. Hermet, M. Goffinet, J. Kreisel, Ph. Ghosez, Phys. Rev. B 75 (2007) 220102.
[22] P. Kharel, S. Talebi, B. Ramachandran, A. Dixit, V.M. Naik, M.B. Sahana, C. Sudakar, R. Naik, M.S.R. Rao, G. Lawes, J. Phys.: Condens. Matter 21 (2009) 036001.
[23] Y. Yang, J.Y. Sun, K. Zhu, Y.L. Liu, J. Chen, X.R. Xing, Physica B 404 (2009) 171.
[24] G.L. Yuan, S.W. Or, H.L.W. Chan, Z.G. Liu, J. Appl. Phys. 101 (2007) 24106.
[25] E. Barsoukov, J.R. MacDonald (Eds.), John Wiley and Sons, Inc., 2005.
[26] A.J. Moulson, J.M. Herbert, Eletroceramics, 2nd Ed., Wiley, New York, 2003.
[27] V.A. Khomchenko, D.A. Kiselev, M. Kopcewicz, M. Maglione, V.V. Shvartsman, P. Borisov, W. Kleemann, A.M.L. Lopes, Y.G. Pogorelov, J.P. Araujo, R.M. Rubinger, N.A. Sobolev, J.M. Vieira, A.L. Kholkin, J. Magn. Magn. Mater. 321 (2009) 1692.